A Regime Map for Granule Formation by Drop Impact on Powder Beds

Heather N. Emady and Defne Kayrak-Talay
School of Chemical Engineering, Purdue University, West Lafayette, IN 47907

James D. Litster
School of Chemical Engineering, Purdue University, West Lafayette, IN 47907

School of Industrial and Physical Pharmacy, Purdue University, West Lafayette, IN 47907

DOI 10.1002/aic.13952

"Tunneling," "Spreading," and "Crater Formation" are the three granule formation mechanisms known to occur when single drops impact static powder beds. To quantify the conditions under which each mechanism will occur, dimensional analysis was performed, and a new regime map was created that plots the powder bed porosity against the modified granular Bond number (Bo_g^*), which is a ratio of the capillary force to the gravitational force acting on a particle. Tunneling occurred for $\mathrm{Bo}_g^* > 65{,}000$ for all values of bed porosity, whereas Spreading and Crater Formation occurred when $\mathrm{Bo}_g^* < 65{,}000$ for all values of bed porosity below the minimum fluidization porosity. The granule formation mechanism regime map provides a useful tool to design and predict wet granulation processes by predicting the granule formation mechanism, and thereby general granule shape, from a few key dimensionless groups involving formulation properties and process parameters that can be calculated a priori. © 2012 American Institute of Chemical Engineers *AIChE J,* 59: 96–107, 2013
Keywords: nucleation, Tunneling, Spreading, Crater Formation, granulation

Introduction

Wet granulation is the formation of granules via the impact of liquid drops onto fine powder. Wetting and nucleation, consolidation and growth, and breakage and attrition are the three rate processes that typically occur in wet granulation.[1] Most granulators use some combination of these processes simultaneously, making it difficult to control each rate process, thereby producing granules of broad size, shape, and density. The concept of regime separated granulation physically isolates each rate process, allowing for narrower product property distributions.[2] Nucleation alone has been demonstrated to produce narrow granule size distributions.[2–4]

Although regime separated granulation promises narrow granule size distributions, it is not clear what kinds of granule shapes can be expected. From her nucleation only formed granules, Hapgood[5] observed a variety of granule shapes, from hemispherical to mushroom shaped. However, no models or set of conditions currently exist for predicting granule shape from single drop formed granules.

Granulation regime maps are available in the literature for both the nucleation and the growth rate processes.[6,7] These tools are invaluable in designing, controlling, and predicting processes based on a few key dimensionless groups. Kayrak-Talay and Litster[8] recently tested the nucleation regime map approach with a complex pharmaceutical formulation in a high shear granulator. By calculating the dimensionless groups from formulation properties and process conditions to place their experiments on the map, they were able to successfully predict the relative spans of the granule size distributions. Although the nucleation regime map defines the conditions under which drop controlled nucleation will occur, it does not provide any details about the variety of behavior and resulting granule attributes occurring within this regime.

In a previous study, "Tunneling," "Spreading," and "Crater Formation" were identified as the three possible granule formation mechanisms that can occur for drop controlled nucleation when single drops are released onto static powder beds.[9] This article will examine each mechanism in more detail with a wide range of additional model powders and experimental conditions. With more data, quantitative assertions can be made for predicting the conditions under which each mechanism, and resulting granule shape, will occur. In this article, a regime map will be proposed and validated that determines the granule formation mechanisms based on dimensionless groups involving powder, liquid, and process properties.

Granule Formation Mechanisms and Proposed Regime Map

The three granule formation mechanisms are known as Tunneling, Spreading, and Crater Formation (Figure 1). Tunneling occurs in loose, cohesive powder beds, where aggregates are sucked into the drop that then tunnels into the bed.

Correspondence concerning this article should be addressed to H. N. Emady at hnemady@gmail.com.

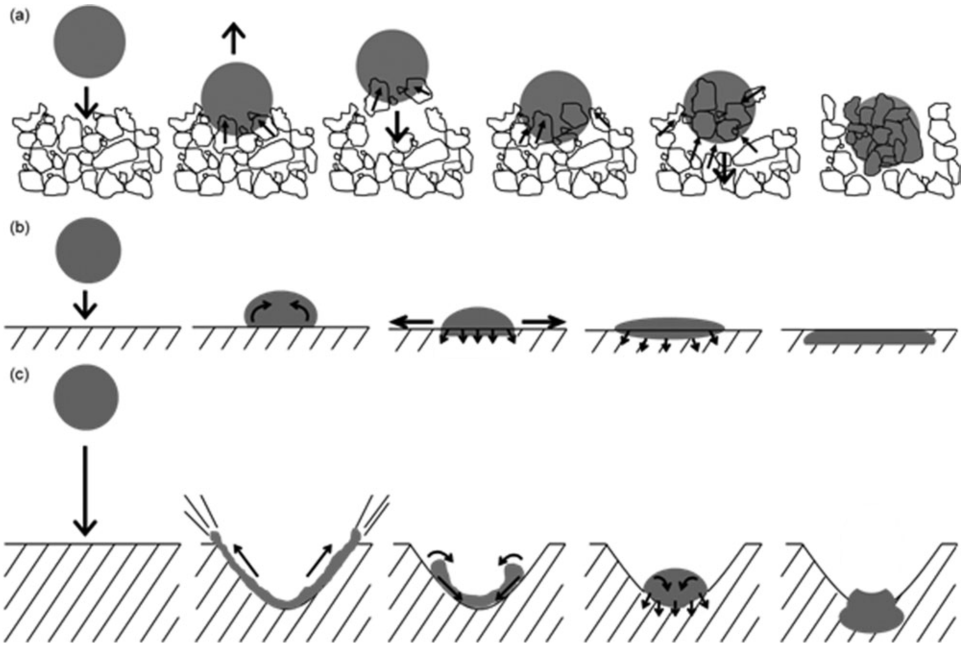

Figure 1. Schematics of the three granule formation mechanisms[9]: (a) Tunneling, (b) Spreading, and (c) Crater Formation.

For coarser powders, granules are formed by Spreading at a low impact velocity, and Crater Formation at a high impact velocity. With Spreading, the drop spreads across the powder bed surface with very shallow capillary penetration. In Crater Formation, the drop impact forms a crater in the powder bed, deforming elastically while picking up particles from the crater, and then penetrates into the bed by capillary action.

A dimensional analysis was performed to determine the relevant dimensionless groups governing single drop granule formation. All the variables involved in single drop granule formation, along with their dimensions, are given in Table 1. The dimensions include mass, M, length, L, and time, T. The force, F, can be expressed in terms of the other variables as $F = MLT^{-2}$.

As a start, the variables are grouped according to well-known dimensionless numbers:

Weber number, which incorporates liquid and process variables

$$We = \frac{d_\mathrm{d} U^2 \rho_\mathrm{l}}{\gamma} \tag{1}$$

Reynolds number, which incorporates liquid and process variables

$$Re = \frac{d_\mathrm{d} U \rho_\mathrm{l}}{\mu} \tag{2}$$

and powder bed porosity, which incorporates powder and process variables

$$\varepsilon = 1 - \frac{\rho_\mathrm{bed}}{\rho_\mathrm{p}} \tag{3}$$

The product properties can be combined into the vertical aspect ratio (V.A.R.), which was defined as a three-dimensional shape descriptor by Emady et al.[9]

$$\mathrm{V.A.R.} = \frac{d_\mathrm{a}}{h_\mathrm{max}} \tag{4}$$

To combine the remaining variables, a dimensionless group relevant in particle–liquid systems, the granular Bond number, is used. Incorporating liquid, powder, and process variables, the granular Bond number is defined as (modified from Nase et al.[10])

$$Bo_\mathrm{g} = \frac{\gamma}{d_{32}^2 \rho_\mathrm{p} g} \tag{5}$$

To include contact angle, Bo_g can be multiplied by cos θ to give

$$Bo_\mathrm{g}^* = \frac{\gamma \cos\theta}{d_{32}^2 \rho_\mathrm{p} g} \tag{6}$$

The quantity in the numerator of Bo_g^*, γ cos θ, is known as the adhesion tension. Bo_g^* is the ratio of the capillary force

Table 1. Variables Involved in Dimensional Analysis

Property	Variable	Dimensions
Liquid	Viscosity, μ	$FL^{-2}T = ML^{-1}T^{-1}$
	Density, ρ_l	ML^{-3}
	Surface tension, γ	$FL^{-1} = MT^{-2}$
	Contact angle, cos θ	–
Powder	Particle density, ρ_p	ML^{-3}
	Surface mean particle diameter, d_{32}	L
Process	Drop diameter, d_d	L
	Drop velocity, U	LT^{-1}
	Powder bed density, ρ_bed	ML^{-3}
	Gravity, g	LT^{-2}
Product	Granule projected area diameter, d_a	L
	Granule maximum vertical height, h_max	L

acting on a particle (of order $d_{32}\gamma\cos\theta$) and the gravitational force acting on the particle (of order $d_{32}^3\rho_p g$). Thus, the Bond number measures the relative magnitude of the cohesive force acting on the particle due to liquid bridges.

The Hausner ratio, which is the tapped density divided by the bulk density, is an indirect measure of dimensionless powder cohesion due to other cohesive forces such as van der Waals and electrostatic forces. Given that the cohesive forces due to liquid bridges between particles are generally at least one order of magnitude greater than those due to van der Waals and electrostatic forces,[11] bulk properties are neglected and Bo_g^* is chosen to represent the cohesive nature of the particles and the particle/liquid interactions. Thus, the dimensional analysis leads to the following proposed relationship

$$\text{V.A.R.} = f(Bo_g^*,\ Re,\ We,\ \varepsilon) \tag{7}$$

Following a regime map approach, each granule formation mechanism will be classified based on the dimensionless groups derived above, and relationships for V.A.R. within each regime will be established.

The process of Tunneling for fine, cohesive powders involves a drop sucking in dry powder aggregates, which will occur when the surface tension driven cohesive force exceeds the weight of the aggregate. Therefore, it is expected that Tunneling will occur at high values of Bo_g^*.

Coarse, free-flowing powders exhibit either a Spreading or a Crater Formation mechanism, depending on the impact conditions. Crater Formation occurs at higher values of both *Re* and *We*. It is also expected that the V.A.R. will be a particularly strong function of *Re* and *We* for both of these mechanisms, as flat disks were observed with Spreading, whereas Crater Formation produced rounder granules.[9]

To construct the regime map, Bo_g^* will be used on one axis to represent the cohesive force, where Tunneling will occur at higher values of Bo_g^* than Spreading or Crater Formation. Bo_g^* should be used in place of Bo_g whenever possible, as it provides more information about the system with the addition of the contact angle. However, Bo_g is a good alternative when contact angle data is not available, provided the system is wetting ($\theta < 90°$). As the difference between Spreading and Crater Formation is due to impact conditions only, these mechanisms will be lumped together when distinguishing the mechanism based on the cohesive force. Also, as Tunneling was found to be independent of impact conditions as well as liquid properties,[9] *Re* and *We* cannot be used to distinguish Tunneling from Spreading/Crater Formation. However, these two groups will be used to distinguish Spreading from Crater Formation, as well as to explain the V.A.R.'s in these regimes.

To further distinguish Tunneling from Spreading/Crater Formation, the bed porosity is a logical choice for the remaining axis on the regime map. Although Tunneling occurs both in its natural loose packed state, as well as upon compression in a more dense bed, the V.A.R. is expected to be a strong function of bed porosity in this regime. Spreading/Crater Formation powders naturally form denser beds, so values of ε will be smaller in this regime.

The proposed regime map of ε vs. Bo_g^* is shown in Figure 2. At high values of Bo_g^*, Tunneling occurs regardless of bed porosity, whereas lower values of Bo_g^* result in Spreading/Crater Formation behavior. Powders within this regime are coarse and naturally form dense powder beds and the only way to make them more porous is to fluidize them, thereby introducing the "Engulfing" regime. The boundary separating Spreading/Crater Formation and Engulfing is the minimum fluidization bed porosity, ε_{mf}. Clear boundaries will be determined, and the existence of the mechanisms will be confirmed by single drop experiments with the wealth of powders presented in this study.

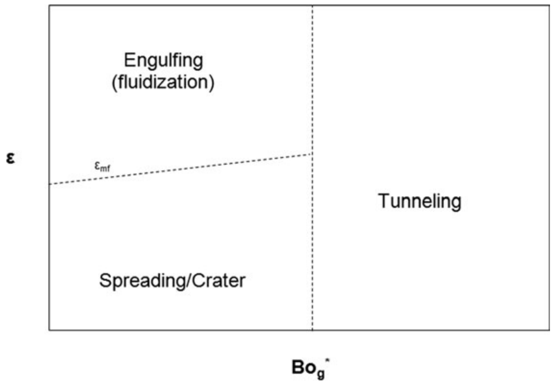

Figure 2. Proposed granule formation mechanism regime map.

Experimental

Materials characterization

Three powders (A1, B, and BM, previously referred to as Powder A, Powder B, and Powder C, respectively) were used in a prior study that identified the granule formation mechanisms.[9] Additional model materials used in this study include 11 refractory inorganic powders supplied by Honeywell and two different sizes of glass ballotini. The powders varied in chemistry, size and size distribution, porosity, and bulk properties. Many of the powders had raw feed as well as milled versions, enabling the study of particle size effects. The powders are named alphabetically, and each milled version is denoted with an "M" following the letter of its corresponding raw feed. For example, B is the raw feed, whereas BM is the milled version of powder B. A number after the powder signifies a physically modified version of the powder, not necessarily by milling. For example, A1, A2, and A3 are all different modifications of powder A.

Particle size and size distribution (Malvern Mastersizer 2000), true particle density (Micromeritics Accupyc II 1340), and bulk and tapped densities (Varian Tapped Density Tester) were measured for each powder. The Hausner ratio was calculated as the tapped density divided by the bulk density. The Geldart classification was decided based on the Hausner ratio.[12] Both the Hausner ratio and the Geldart classification qualitatively classify the flowability of powder. Hausner ratios less than 1.25 are Geldart A powders that are aeratable and easy to fluidize, whereas those greater than 1.4 are Geldart C powders that are cohesive and difficult to fluidize. The powders with Hausner ratios between 1.25 and 1.4 are Geldart AC powders that are transitional.[12] The powder characterization summary, with 95% confidence intervals, is given in Table 2. The values reported are the averages of three to four replicates.

The primary liquid used in experiments was distilled water with a 22-gauge needle. Other liquids and drop sizes were used for additional experiments, particularly for the Crater

Table 2. Physical Properties of Model Powders

Powder	Surface Mean, d_{32} (μm)	True particle Density, ρ_s (g/cm^3)	Pore Volume,* V_p (cm^3/g)	Apparent Particle Density, $\rho_p = \rho_s/(1 + V_p\rho_s)$ (g/cm^3)	Bulk Density, ρ_B (g/cm^3)	Tapped Density, ρ_T (g/cm^3)	Hausner Ratio, ρ_T/ρ_B	Geldart Classification
A1	2.97 ± 0.01	2.495 ± 0.004	0.83 ± 0.01	0.812 ± 0.007	0.30 ± 0.03	0.523 ± 0.003	1.7 ± 0.2	C
A2	9.37 ± 0.06	2.488 ± 0.004	0.94 ± 0.01	0.745 ± 0.006	0.305 ± 0.004	0.386 ± 0.004	1.27 ± 0.02	AC
A3	2.63 ± 0.08	4.08 ± 0.01	0.01 ± 0.01	3.9 ± 0.1	0.44 ± 0.02	0.68 ± 0.01	1.55 ± 0.07	C
B	15 ± 1	2.479 ± 0.002	0.45 ± 0.01	1.17 ± 0.01	0.78 ± 0.03	1.00 ± 0.008	1.29 ± 0.05	AC
BM	3.6 ± 0.2	2.5431 ± 0.0007	0.42 ± 0.01	1.23 ± 0.02	0.51 ± 0.03	0.87 ± 0.02	1.7 ± 0.1	C
C	25.9 ± 0.2	2.1992 ± 0.0005	0.84 ± 0.01	0.774 ± 0.006	0.430 ± 0.002	0.542 ± 0.006	1.26 ± 0.01	AC
CM1	5.05 ± 0.04	2.189 ± 0.002	0.76 ± 0.01	0.825 ± 0.007	0.2074 ± 0.0002	0.426 ± 0.005	2.05 ± 0.02	C
CM2	4.53 ± 0.03	2.179 ± 0.001	0.73 ± 0.01	0.839 ± 0.007	0.204 ± 0.009	0.409 ± 0.006	2.00 ± 0.09	C
D	2.74 ± 0.08	1.962 ± 0.002	0.35 ± 0.01	1.16 ± 0.01	0.328 ± 0.008	0.49 ± 0.01	1.48 ± 0.05	C
DM	1.51 ± 0.01	1.9403 ± 0.0008	0.36 ± 0.01	1.15 ± 0.01	0.343 ± 0.009	0.55 ± 0.02	1.59 ± 0.06	C
E	3.56 ± 0.02	1.8630 ± 0.0009	0.42 ± 0.01	1.04 ± 0.01	0.38 ± 0.02	0.600 ± 0.005	1.57 ± 0.08	C
EM	2.88 ± 0.05	1.857 ± 0.001	0.42 ± 0.01	1.05 ± 0.01	0.381 ± 0.008	0.612 ± 0.005	1.61 ± 0.04	C
F	5.5 ± 0.1	2.351 ± 0.002	0.45 ± 0.01	1.14 ± 0.01	0.31 ± 0.01	0.540 ± 0.006	1.74 ± 0.08	C
FM	4.96 ± 0.01	2.380 ± 0.003	0.42 ± 0.01	1.19 ± 0.01	0.15 ± 0.01	0.282 ± 0.009	1.9 ± 0.2	C
G1	261 ± 2	2.4877 ± 0.0001	0	2.4877 ± 0.0001	1.50 ± 0.01	1.600 ± 0.002	1.07 ± 0.01	A
G2	67.5 ± 0.7	2.4639 ± 0.0002	0	2.4639 ± 0.0002	1.4 ± 0.2	1.50 ± 0.06	1.1 ± 0.1	A

*Data from nitrogen adsorption, performed by Honeywell.

Formation regime. Surface tension was measured by the Wilhemy plate technique (Kruss Tensiometer). The theoretical drop diameter was calculated from a force balance between surface tension and gravity force of the drop in the dripping regime. The liquid binder properties, with 95% confidence intervals, are given in Table 3.

Wettability is an essential property of any powder/liquid system that has a significant impact on the mechanism that will occur when a drop penetrates into a powder bed. To quantify wettability, the contact angle was measured for each powder/liquid combination through the Washburn method (Kruss Tensiometer). The Washburn method is only valid for spontaneously wetting systems, where the contact angle is between 0 and 90°.

The capillary constants as well as the contact angles for each powder/liquid sample, with 95% confidence intervals, can be found in Table 4.

The granules were analyzed using the prism imaging technique that was introduced in a previous study.[9] Individual granules were placed in the prism setup, capturing both the top and the side views of the granule in 1–2 microscope images, depending on the size of the granule. The images were subsequently analyzed with Adobe Photoshop CS4 with the Fovea Pro 4.0 plug-in to obtain the projected area diameter, d_a, of each granule. Maximum granule height, h_{max}, was measured manually with UTHSCSA ImageTool 3.00. The vertical aspect ratio (V.A.R.) was calculated as the ratio of the projected area diameter to the maximum granule height. The V.A.R. has been shown to be an accurate representation of granule shape, because it captures all three dimensions of the granule.[9]

Experimental methods

A Petri dish method was previously used to prepare the powder beds, where powder was lightly sieved through a 2.00-mm sieve and leveled off with a ruler.[9] In this study, an alternative powder bed preparation method was investigated using the Freeman FT4 Powder Rheometer in an attempt to get more reproducible powder bed porosities, as well as to eliminate the human error present with the Petri dish preparation technique. A 50-mm diameter split vessel was assembled with a 160-mL vessel on the bottom and an 85-mL vessel on the top. Enough powder was poured into the split vessel to ensure the powder level would stay above the split line for the duration of the bed conditioning. In a conditioning step, a blade rotated clockwise while moving down through the bed (see Figure 3, left). Conditioning is expected to reduce macrovoids and create a reproducible powder bed structure. Seven conditioning steps were performed for each powder bed. To vary the porosity of the powder beds, the blade was replaced by a solid piston after conditioning, placing different amounts of forces on the powder bed to compact it. After the bed was conditioned and sometimes compacted, the vessel was split to give an even surface for single drop experiments (see Figure 3, right). The same single drop high-speed camera setup was used for the powder beds prepared in the Freeman and those prepared in Petri dishes (see Emady et al.[9] for details).

Table 3. Liquid Binder Properties

Liquid	Viscosity (mPa s)	Density (g/mL)	Surface Tension (mN/m)	Syringe Needle Gauge	Drop Diameter (mm)
Distilled water	1	1	72.0 ± 0.3	33	1.70
Distilled water	1	1	72.0 ± 0.3	22	2.64
Silicone oil	9.3*	0.93*	20.2 ± 0.2	14	2.71
Silicone oil	96*	0.96*	20.9 ± 0.7	14	2.77
Ethanol	1.2[†]	0.8[‡]	23.45 ± 0.03	22	1.95
40% glycerin	3.7[†]	1.1[‡]	61.76 ± 0.05	22	2.42
50% glycerin	6.0[†]	1.1[‡]	59.5 ± 0.3	22	2.36

*Data from Sigma–Aldrich.
[†] Literature data.
[‡] Data from the Kruss Tensiometer.

Table 4. Contact Angles and Capillary Constants for All Powder/Liquid Combinations

Powder	Capillary Constant with Hexane (cm^5)	Liquid	Contact Angle (°)
A1	2.7 ± 0.1E−6	Distilled water	72 ± 2
		9.3 mPa s silicone oil	8 ± 19
		96 mPa s silicone oil	0*
A2	6.6 ± 0.8E−6	Distilled water	59 ± 7
A3	7.5 ± 0.5E−6	Distilled water	64 ± 4
B	4.4 ± 0.1E−6	Distilled water	84.7 ± 0.1
		9.3 mPa s silicone oil	0*
		96 mPa s silicone oil	0*
		Ethanol	70 ± 2
		40% glycerin	84.6 ± 0.9
		50% glycerin	84 ± 2
BM	1.6 ± 0.1E−6	Distilled water	81 ± 1
C	1.05 ± 0.07E−5	Distilled water	38 ± 6
CM1	2.6 ± 0.3E−6	Distilled water	52 ± 4
CM2	2.2 ± 0.2E−6	Distilled water	49 ± 8
D	5.0 ± 0.4E−6	Distilled water	38 ± 9
DM	3.9 ± 0.4E−6	Distilled water	64 ± 21
E	2.8 ± 0.1E−6	Distilled water	63 ± 5
EM	2.5 ± 0.2E−6	Distilled water	51 ± 3
F	4.3 ± 0.3E−6	Distilled water	N/A†
FM	5.6 ± 0.1E−6	Distilled water	N/A†
G1	2.6 ± 0.6E−5	Distilled water	71 ± 3
G2	1.9 ± 0.2E−5	Distilled water	59 ± 5

*Measurements gave $\cos \theta > 1$, indicating better wetting than hexane.
†Washburn test inappropriate for fibrous clay particles (Kruss technician, personal communication).

Single drops were released onto the prepared powder beds, and high-speed video imaging captured the drop impact and penetration.

Experimental design

The aim of this study is to determine the boundaries of the regime map between the Spreading/Crater Formation and Tunneling regimes. In addition to the experimental data in our other studies (Kayrak-Talay et al., in preparation),[9,13] 13 more powders were characterized and tested in this study to be used in the validation. The list of powders and the experimental conditions are given in Table 5 with the granule characterization results.

Drops were released from 0.5 cm onto powder beds consisting of each of the 13 new powders. The Tunneling mechanism is known to be insensitive to the liquid properties and drop release height.[9] If the mechanism was Tunneling, no further drop heights were tested. However, the dependence of the Tunneling mechanism on the bed porosity and bed structure was investigated through different powder bed preparation techniques with the Petri dish and Freeman Rheometer.

If the mechanism was Spreading at 0.5 cm, experiments were performed at 30 cm to capture the Crater Formation mechanism. Powder A2 was tested at additional drop heights because it appeared to have transitional Spreading/Crater Formation behavior. Powder B was tested with various drop heights and liquids to examine granule shape in the Crater Formation regime.

Results: Granule Formation Mechanisms and Morphology

High-speed videos were examined to determine the granule formation mechanism, and the granules were analyzed using the prism imaging technique.[9]

Granule shape was characterized by the vertical aspect ratio (V.A.R.), which is the ratio of the projected area diameter, d_a, to the maximum granule height, h_{max}. In a previous study, the V.A.R. was found to be the most discriminatory representation of granule shape, capturing all three dimensions of the granule.[9] It was also found that each mechanism generates distinct granule shapes. The Tunneling mechanism always produced round granules with V.A.R.'s close to one, whereas the Spreading mechanism always produced flat disks with high V.A.R.'s. However, the Crater Formation mechanism produces granules that are dependent on liquid properties and process conditions. Similar observations were made in this study over the full range of powders and liquids studied.

The granule characterization data, with V.A.R., Bo_g^*, and corresponding formation mechanism, are given in Table 5.

Figure 3. Freeman powder bed preparation setup.

The powder is conditioned with a blade to create uniformity within the bed (left). The vessel is then split to create a smooth surface for single drop experiments (right). [Color figure can be viewed in the online issue, which is available at wileyonlinelibrary.com.]

Table 5. Granule Characterization

Powder	Liquid	Powder Bed Porosity, ε	Drop Height (cm)	V.A.R.	Mechanism	Bo_g^*
A1[†]	Distilled water (22G)	0.68 ± 0.01	0.5	1.05 ± 0.03	Tunneling	3.17E5
A1	Distilled water (22G)	0.576 ± 0.005	0.5	1.07 ± 0.03	Tunneling	3.17E5
A1	Distilled water (22G)	0.498	0.5	1.20 ± 0.06	Tunneling	3.17E5
A1	Distilled water (22G)	0.434	0.5	1.24 ± 0.07	Tunneling	3.17E5
A1[†]	Distilled water (22G)	0.33	0.5	1.26 ± 0.06	Tunneling	3.17E5
A1[†]	Distilled water (22G)	0.68 ± 0.01	30	1.07 ± 0.02	Tunneling	3.17E5
A1[†]	9.3 mPa s silicone oil	0.68 ± 0.01	0.5	1.08 ± 0.04	Tunneling	2.85E5
A1[†]	9.3 mPa s silicone oil	0.68 ± 0.01	30	1.10 ± 0.04	Tunneling	2.85E5
A1[†]	96 mPa s silicone oil	0.68 ± 0.01	0.5	1.08 ± 0.03	Tunneling	2.98E5
A2	Distilled water (22G)	0.562 ± 0.002	0.5	1.42 ± 0.05	Spreading[‡]	5.79E4
A2	Distilled water (22G)	0.562 ± 0.002	5	1.11 ± 0.03	Crater Formation	5.79E4
A2	Distilled water (22G)	0.562 ± 0.002	10	1.11 ± 0.05	Crater Formation	5.79E4
A2	Distilled water (22G)	0.562 ± 0.002	20	1.14 ± 0.03	Crater Formation	5.79E4
A2	Distilled water (22G)	0.562 ± 0.002	30	1.7 ± 0.4	Crater Formation[§]	5.79E4
A3	Distilled water (22G)	0.878 ± 0.004	0.5	1.3 ± 0.1	Tunneling	1.19E5
B[†]	Distilled water (22G)	0.33 ± 0.02	0.5	2.33 ± 0.16	Spreading	2.58E3
B	Distilled water (33G)	0.33 ± 0.02	10	1.21 ± 0.05	Crater Formation	2.58E3
B	Distilled water (22G)	0.33 ± 0.02	10	1.37 ± 0.04	Crater Formation	2.58E3
B	Distilled water (33G)	0.33 ± 0.02	20	1.19 ± 0.03	Crater Formation	2.58E3
B	Distilled water (22G)	0.33 ± 0.02	20	1.33 ± 0.03	Crater Formation	2.58E3
B	Distilled water (33G)	0.33 ± 0.02	30	1.13 ± 0.03	Crater Formation	2.58E3
B[†]	Distilled water (22G)	0.33 ± 0.02	30	1.22 ± 0.06	Crater Formation	2.58E5
B[†]	9.3 mPa s silicone oil	0.33 ± 0.02	0.5	2.73 ± 0.31	Spreading	7.83E3
B[¶]	9.3 mPa s silicone oil	0.33 ± 0.02	10	2.16 ± 0.08	Crater Formation	7.83E3
B[¶]	9.3 mPa s silicone oil	0.33 ± 0.02	30	1.92 ± 0.10	Crater Formation	7.83E3
B[¶]	9.3 mPa s silicone oil	0.33 ± 0.02	50	1.70 ± 0.06	Crater Formation	7.83E3
B[†]	96 mPa s silicone oil	0.33 ± 0.02	0.5	2.58 ± 0.13	Spreading	8.10E3
B[†]	96 mPa s silicone oil	0.33 ± 0.02	30	2.47 ± 0.16	Crater Formation	8.10E3
B[¶]	Ethanol	0.33 ± 0.02	10	1.65 ± 0.07	Crater Formation	9.55E3
B[¶]	Ethanol	0.33 ± 0.02	30	1.33 ± 0.02	Crater Formation	9.55E3
B[¶]	40% glycerin	0.33 ± 0.02	30	1.59 ± 0.06	Crater Formation	2.63E3
B[¶]	50% glycerin	0.33 ± 0.02	30	1.75 ± 0.05	Crater Formation	2.92E3
BM[†]	Distilled water (22G)	0.55	0.5	1.15 ± 0.04	Tunneling[‡]	7.21E4
BM	Distilled water (22G)	0.496 ± 0.006	0.5	1.28 ± 0.08	Tunneling[‡]	7.21E4
BM[†]	Distilled water (22G)	0.55	30	1.21 ± 0.09	Tunneling[‡]	7.21E4
C	Distilled water (22G)	0.40 ± 0.01	0.5	1.75 ± 0.09	Spreading	1.12E4
C	Distilled water (22G)	0.40 ± 0.01	30	1.3 ± 0.1	Crater Formation	1.12E4
CM1	Distilled water (22G)	0.667	0.5	1.06 ± 0.03	Tunneling	2.15E5
CM2	Distilled water (22G)	0.690	0.5	1.07 ± 0.04	Tunneling	2.80E5
D	Distilled water (22G)	0.715	0.5	1.15 ± 0.07	Tunneling	6.65E5
DM	Distilled water (22G)	0.693	0.5	1.19 ± 0.04	Tunneling	1.23E6
E	Distilled water (22G)	0.571	0.5	1.22 ± 0.08	Tunneling	2.53E5
EM	Distilled water (22G)	0.577	0.5	1.09 ± 0.04	Tunneling	5.31E5
F	Distilled water (22G)	0.794	0.5	1.20 ± 0.04	Spreading[‡]	4.46E3
F	Distilled water (22G)	0.673 ± 0.007	0.5	1.36 ± 0.06	Spreading[‡]	4.46E3
F	Distilled water (22G)	0.673 ± 0.007	30	1.16 ± 0.05	Crater Formation[‡]	4.46E3
FM	Distilled water (22G)	0.833	0.5	1.10 ± 0.03	Tunneling	6.57E3
G1	Distilled water (22G)	0.38 ± 0.01	0.5	1.87 ± 0.04	Spreading	1.41E1
G1	Distilled water (22G)	0.38 ± 0.01	30	2.24 ± 0.06	Crater Formation[§]	1.41E1
G2	Distilled water (22G)	0.42 ± 0.01	0.5	1.90 ± 0.12	Spreading	3.37E2
G2	Distilled water (22G)	0.42 ± 0.01	30	1.54 ± 0.07	Crater Formation	3.37E2

[†] Result from Emady et al.[9]
[‡] Exhibits transitional behavior—possibly on the border between Tunneling and Spreading/Crater Formation.
[§] After spreading upon impact, the drop does not retract, or only partially retracts.
[¶] Result from Kayrak-Talay et al. (in preparation).

The Tunneling granules were relatively round, with V.A.R.'s in the range of 1.05–1.3. Examples of granules formed by Tunneling are given in Figure 4. The granules are generally spherical, but some have protrusions or cavities. Powders A1, CM1, and CM2 are the most spherical (lowest V.A.R.'s), but they have some protrusions. Powders BM and FM form mushroom-shaped granules.

The Spreading granules were all flat disks, as expected, with V.A.R.'s in the range of 1.42–2.73. Examples of granules formed by Spreading are given in Figure 5.

The shape of the Crater Formation granules varied with process conditions, as expected, with V.A.R.'s in the range of 1.11–2.47. Examples of granules formed by Crater Formation are given in Figure 6. As water was the only liquid used in the selected images, drop impact velocity was the distinguishing variable. Although Crater Formation granules are generally more round than Spreading granules, the V.A.R.'s vary greatly with drop height, as shown by the A2 granules.

Unusual granule formation behavior

Powder F displayed very unusual behavior. Initially, the drop appeared to penetrate the powder bed via a Spreading or Crater Formation mechanism. However, after about 2 s, a crack appeared in the powder bed surrounding the drop, suggesting the powder bed was failing in tension as a result of the capillary pressure acting on the bed (see Figure 7). The

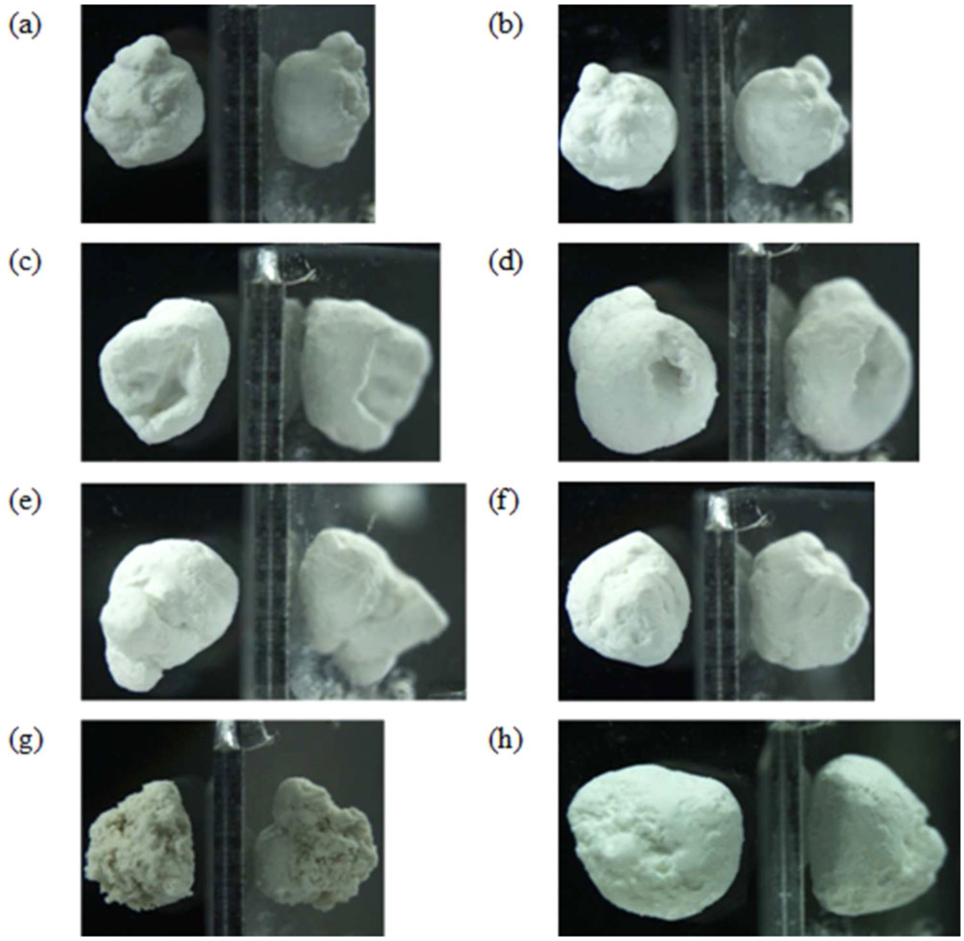

Figure 4. Images of granules formed via Tunneling: from left to right, starting at the top: powders (a) CM1, (b) CM2, (c) D, (d) DM, (e) E, (f) EM, (g) FM, and (h) A3.

Each granule was formed from a single water droplet (2.64 mm in diameter) that was released from 0.5 cm. The granule size is of the same order as the drop size. [Color figure can be viewed in the online issue, which is available at wileyonlinelibrary.com.]

complexity in bed structure is most likely due to interlocking behavior of the fibrous particles. Thus, rather than a bed of loose aggregates that can be sucked individually into the drop, the bed behaves as an interlocked mat that fails in tension if the liquid surface forces are large enough.

At a drop height of 0.5 cm, granules were formed that had V.A.R.'s of either 1.36 or 1.61, depending on bed porosity (see Table 5 and Figure 8a). The V.A.R. significantly improved to 1.16 when the drop height was raised to 30 cm (see Table 5 and Figure 8b). This significant improvement in V.A.R. on increasing the drop height is indicative of transitioning from Spreading to Crater Formation. However, due to the additional behavior of the granule pulling away from the bed after drop penetration, powder F cannot be placed confidently into a regime.

Validation of the Granulation Formation Mechanism Regime Map

To validate the regime map, the proposed dimensionless groups, ε and Bo_g^*, were calculated for each experiment and compared to the mechanisms observed through high-speed video analysis. The regime map, with all of the experimental data, is given in Figure 9.

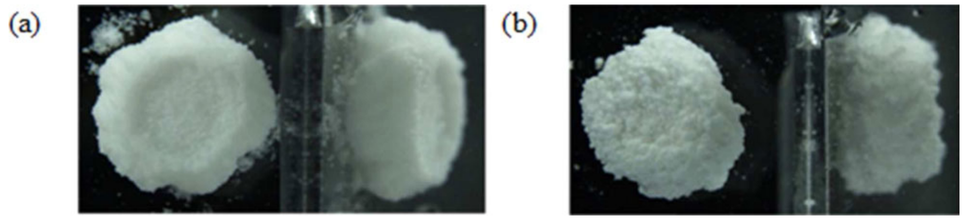

Figure 5. Images of granules formed via Spreading: powders (a) C and (b) A2.

Each granule was formed from a single water droplet (2.64 mm in diameter) that was released from 0.5 cm. The granule size is of the same order as the drop size. [Color figure can be viewed in the online issue, which is available at wileyonlinelibrary.com.]

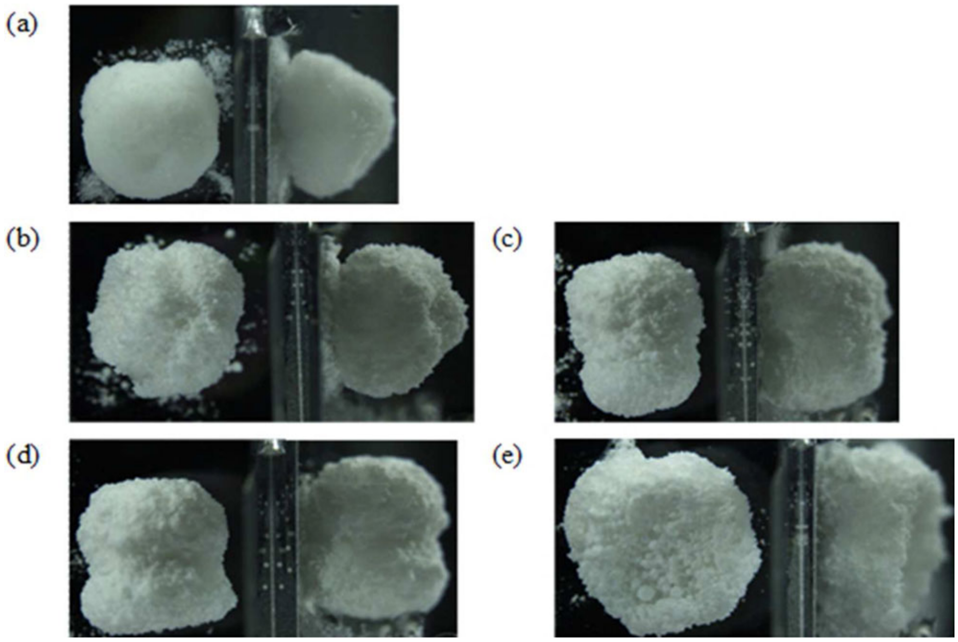

Figure 6. Images of granules formed via Crater Formation: from left to right, starting at the top: powders (a) C from 30 cm, (b) A2 from 5 cm, (c) A2 from 10 cm, (d) A2 from 20 cm, and (e) A2 from 30 cm.

Each granule was formed from a single water droplet (2.64 mm in diameter). The granule size is of the same order as the drop size. [Color figure can be viewed in the online issue, which is available at wileyonlinelibrary.com.]

The $\varepsilon_{\mathrm{mf}}$ boundary between the Spreading/Crater Formation and Engulfing regimes was calculated from an empirical correlation based on the particle size[14]

$$\varepsilon_{\mathrm{mf}} = 0.77(d_{32})^{-0.124} \tag{8}$$

Powders A2 and BM determined the boundary between Spreading/Crater Formation and Tunneling, with the boundary being around $Bo_g^* = 65{,}000$. Powder BM exhibits distinct Tunneling behavior, but the granules formed are mushroom shaped rather than round, which explains why this powder is near the boundary. Powder A2 is definitely in the Spreading/Crater Formation regime, but the granule shape displays a sensitivity to drop height that is different from the other powders in this regime (see Table 5 and Figures 5 and 6). Therefore, it makes sense that powder A2 would be on the boundary just inside the Spreading/Crater Formation regime.

Powders F and FM are the only powders not displayed on the regime map. These clay particles are fibrous, resulting in very high bed porosities. Bo_g^* could not be calculated due to the difficulty in measuring the powder/liquid contact angle. Powder FM exhibited Tunneling and should fall into this regime if a more accurate contact angle could be measured. However, powder F formed a unique bed structure where the fibrous particles interlock, which is inherently different from the other powder beds that are comprised of dry powder aggregates or single particles. It showed unique behavior with the granule pulling away from the surrounding powder bed after drop penetration (see Figures 7 and 8). We

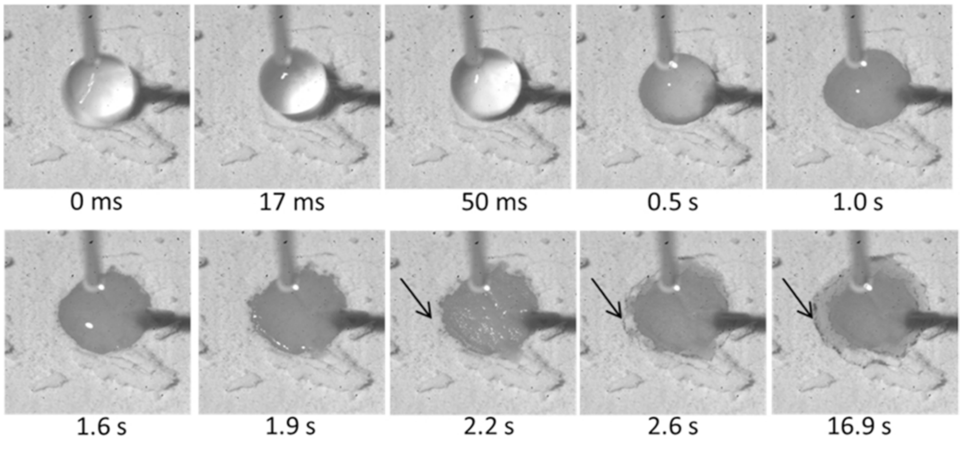

Figure 7. Video sequence of a water droplet impacting and penetrating into powder F from a drop height of 0.5 cm.

The drop spreads and retracts, then spreads back again, exhibiting traits of the Spreading mechanism. However, the granule later pulls away from the surrounding powder. [Color figure can be viewed in the online issue, which is available at wileyonlinelibrary.com.]

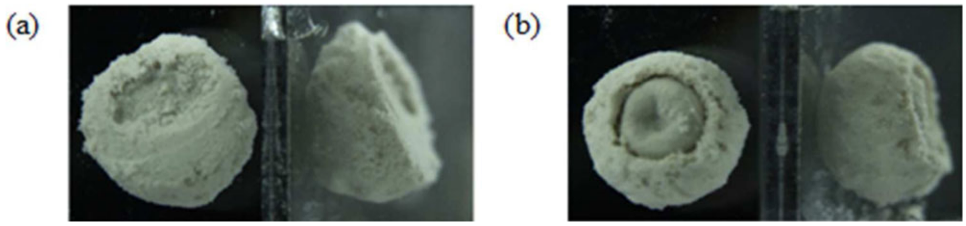

Figure 8. Images of powder F granules from water drops (2.64 mm in diameter) released from (a) 0.5 cm and (b) 30 cm.

The granule size is of the same order as the drop size. [Color figure can be viewed in the online issue, which is available at wileyonlinelibrary.com.]

conclude that the regime map is not applicable to fibrous materials.

It is remarkable that 14 powders, over a range of bed porosities from 0.33 to 0.878 and Bo_g^* values from 14.1 to 1.23E6, fit clearly into either the Tunneling or the Spreading/Crater Formation regime.

Boundaries and granule properties in the Spreading/Crater Formation regime

The data in the regime map confirm that Spreading/Crater Formation occurs at low values of Bo_g^*, with values ranging from 14.1 for powder G1 to 5.79E4 for powder A2. The Spreading/Crater Formation mechanism will occur in this low Bo_g^* region at low values of bed porosity (0.33–0.562), which are below the minimum fluidization porosity.

V.A.R.'s for Spreading granules range from 1.42 to 2.73, whereas those for Crater Formation granules range from 1.11 to 2.47. To quantify the difference between these two regimes, the Reynolds and Weber numbers were calculated (see Eqs. 1 and 2). A plot of *Re* vs. *We* for all conditions identified as Spreading/Crater Formation is shown in Figure 10. Crater Formation occurs at relatively high values of *We* ($\geq$33), and *Re* does not distinguish between the mechanisms. As the main difference between *We* and *Re* is that *We* incorporates surface tension whereas *Re* incorporates viscosity, this indicates that viscosity plays no role in determining the mechanism, while surface energy is important. In the Crater Formation regime, the impact energy greatly exceeds the surface energy of the drop.

To examine trends in granule shape between the Spreading and Crater Formation regimes, V.A.R. is plotted against *We* in Figure 11. The roundest granules (lowest V.A.R.) occur at Weber numbers just high enough to be in the crater regime. Within the crater regime, V.A.R. broadly increases with *We*, but there is considerable scatter in the data. Viscosity may also affect granule shape in this regime and for coarse powders there may be an optimum impact energy, beyond which the liquid penetrates the bed before full retraction of the drop. Further analysis of the complex phenomena in the crater regime is given in Ref. 13 and Kayrak-Talay et al. (in preparation).

Granule properties in the Tunneling regime

The data in the regime map confirm that Tunneling occurs at high values of Bo_g^*, with values ranging from 7.21E4 for powder BM to 1.23E6 for powder DM. The Tunneling

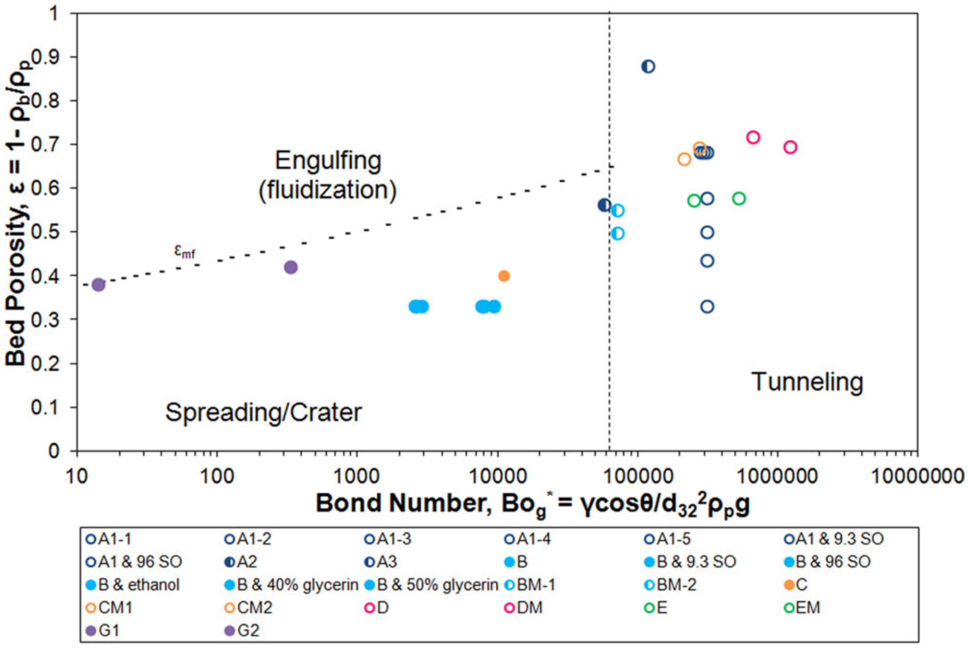

Figure 9. Granule formation mechanism regime map.

The filled dots indicate Spreading/Crater Formation, the open dots indicate Tunneling, and the partially filled dots indicate transitional behavior, with the mostly filled dot (A2) leaning toward Spreading/Crater Formation and the mostly empty dots (A3 and BM) leaning toward Tunneling. [Color figure can be viewed in the online issue, which is available at wileyonlinelibrary.com.]

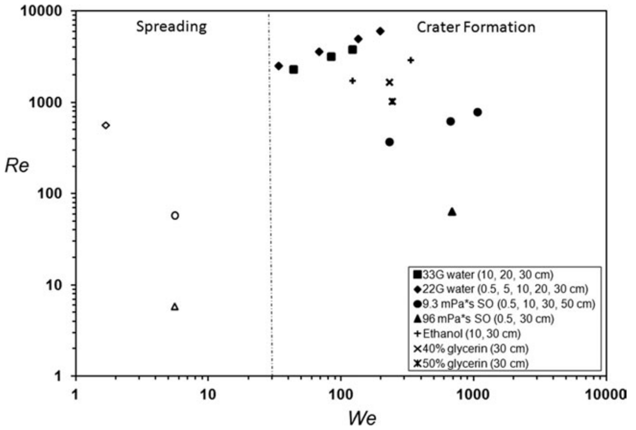

Figure 10. *Re* vs. *We* for Spreading and Crater Formation granules.

The open points indicate Spreading, whereas the filled points indicate Crater Formation.

mechanism will occur in this high Bo_g^* region independent of bed porosity, as shown by the wide range of bed porosities (0.33–0.878) tested in this region.

Granules formed via Tunneling have V.A.R.'s ranging from 1.05 to 1.3 (see Table 5). V.A.R. is not a function of Bo_g^*, as can be seen in Figure 12. In fact, powder A1, at a granular Bond number of 3.17E5, forms granules with V.A.R.'s varying from 1.05 to 1.26 for different powder bed porosities. Therefore, V.A.R. is expected to be dependent on bed porosity. A plot of V.A.R. vs. bed porosity for all powders in the Tunneling regime is given in Figure 13.

V.A.R. generally decreases with increasing bed porosity, but there is scatter in the data for different powder types, and the bed preparation procedure also affects the granule shape (see Figure 13). Powder A1 beds were prepared at a number of different porosities, and the V.A.R. improves (decreases) with increasing powder bed porosity for a given bed preparation method. We expect a similar trend will hold for other powders.

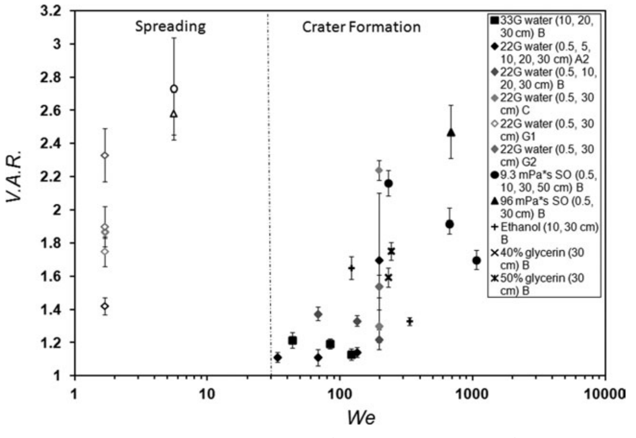

Figure 11. V.A.R. vs. *We* for Spreading and Crater Formation granules.

The open points indicate Spreading, whereas the filled points indicate Crater Formation.

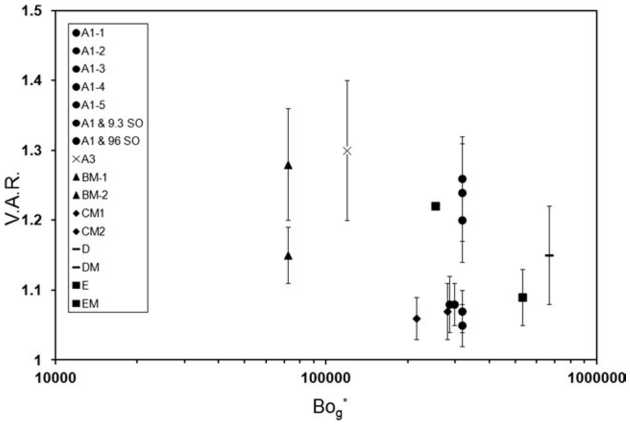

Figure 12. V.A.R. vs. Bo_g^* for Tunneling granules.

Powders A1 and BM were tested with both bed preparation methods. With powder BM, only the "loose packed" versions of each method were tested: loose packed Petri dish and seven conditionings in the Freeman. Powder A1 was tested with different levels of compaction within each method. With a given method, the V.A.R. improves with increasing bed porosity, and the loose packed version produces the roundest granules, as indicated by the furthest right point on either connected line in Figure 13. Within experimental error, the granule shape (V.A.R.) was independent of preparation technique for a given bed porosity. However, the Petri dish technique can give higher bed porosities. It is expected that most powder beds used in continuous processing would be naturally loose packed, as powder would be poured into the system without the use of any compaction or conditioning tool, as can be envisioned with Wildeboer's conveyor belt nucleation apparatus.[2] Therefore, it is promising that round granules would be achieved with the Tunneling mechanism in industrial processes.

Both powders BM and A3 exhibited the highest V.A.R.'s of 1.28 and 1.3, respectively, when prepared with the Freeman Rheometer conditioning. Powder BM granules were mushroom shaped, whereas powder A3 granules were relatively flat (see Figure 4). Powder A3 also exhibits anomalous behavior with a high V.A.R., despite the high porosity of the bed prepared using the Freeman. The reason for higher V.A.R.'s and unusual shapes could stem from the fact that both of these powders lie closest to the border between

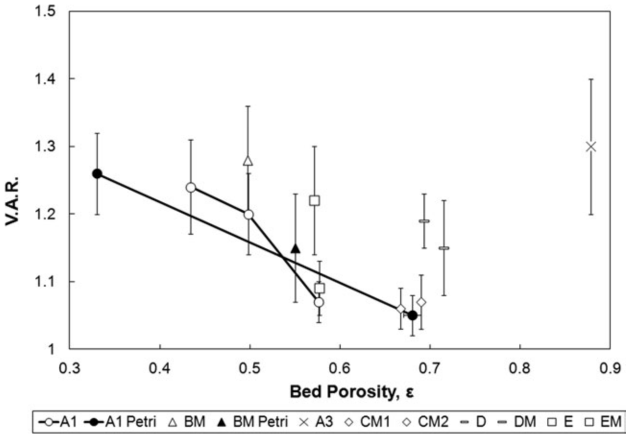

Figure 13. V.A.R. comparison for Tunneling granules resulting from both powder bed preparation methods.

Those prepared with the Freeman are marked as open points, whereas Petri dish formed granules are filled points.

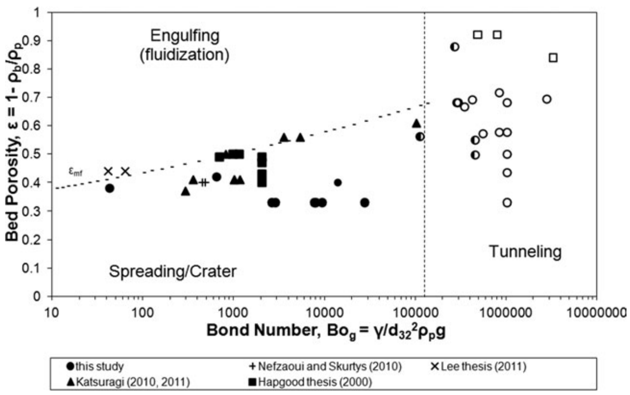

Figure 14. Granule formation mechanism regime map with literature values.

The filled points indicate Spreading/Crater Formation, the open dots indicate Tunneling, and the partially filled dots indicate transitional behavior.

Tunneling and Spreading/Crater Formation (see Figure 9). Although these powders exhibit Tunneling behavior, lying near the border could signify that a region exists here where the powders have shapes differing from the typical spherical Tunneling formed granules.

Engulfing regime

Although the Engulfing regime was not tested in this study, free-flowing powders have the potential to give round granules when fluidized. When a drop impacts fluidized powder, it is expected to have a mechanism similar to Tunneling, where powder is pulled into the drop from all sides, which is known to produce round granules. The Engulfing mechanism has been observed in the fluidized bed granulation literature, but little detail has been given on the mechanism.[4,15]

Comparison with literature

A survey of the literature on single drop granule formation allowed the compilation of data relevant to the regime map. Most authors did not measure contact angle and, therefore, Bo_g is used in place of Bo_g^* to place the data on the regime map, given in Figure 14. Four different studies provided enough information to calculate the dimensionless groups, and subsets of these data were placed on the regime map only if enough information on the mechanisms was given in the form of high-speed video images, granule shape images, or observations.[5,16–19] Three additional studies qualitatively confirmed the mechanisms, but not enough information was given to calculate the dimensionless groups.[20–22] Detailed information of all relevant quantitative and qualitative literature data is given in Emady's thesis.[23] Despite the absence of contact angle, the regime map effectively accounts for the behavior seen in the literature.

Nefzaoui and Skurtys[16] and Lee[17] did experiments on large glass ballotini ($d_{32} \geq 81$ μm), so all of their data should fall in the Spreading/Crater Formation regime. The high-speed video images provided by these authors clearly depict the Crater Formation mechanism.[16,17] Therefore, data from each of these references can be placed on the regime map in the Spreading/Crater Formation regime with confidence (see Figure 14).

Katsuragi[18] provided the most information about granule formation mechanisms with his crater shape map. His map only incorporated SiC particles and did not include the glass ballotini that he tested in a later article.[19] At SiC particle sizes of 4 and 8 μm, he reported a "sink" mechanism that was independent of drop height up to 10 cm, which might indicate Tunneling behavior, but based on high-speed video images, it is possible that this mechanism could in fact be Spreading.[19] As the mechanism is unclear, all data involving the 4 and 8 μm SiC particles are not included on the regime map in Figure 14. The rest of the SiC particles exhibited "ring" and "bump" behavior, which most likely resemble Spreading/Crater Formation. The high-speed video images for the large SiC particles ($d_{32} \geq 14$ μm) as well as for all the glass ballotini show Spreading/Crater Formation behavior[19] and are marked as such on the regime map in Figure 14.

In her thesis, Hapgood[5] provided a lot of data and made many qualitative observations about granule shape, which can be partially linked to the regime map. She noted that Spreading did not occur in the formation of her ZnO and TiO_2 granules ($d_{32} \leq 1.25$ μm), so they were most likely formed via Tunneling. The glass ballotini ($d_{32} = 29.61$ μm) with PEG200 and PEG600, UQ lactose ($d_{32} = 64.43$ μm) with water and PEG600, as well as coarse UQ lactose ($d_{32} = 69.66$ μm) with water all formed hemispheres or flat disks, which indicate Spreading/Crater Formation granules. The remainder of her lactose powders formed variations of mushroom shapes at different conditions, which could designate transitional behavior and therefore are not included on the regime map. On the regime map in Figure 14, ZnO and TiO_2 are marked with open points for Tunneling, and the glass ballotini as well as the relevant lactose conditions are marked with closed points for Spreading/Crater Formation.

Agland and Iveson,[20] Marston et al.,[21] and Delon et al.[22] did not provide enough information to calculate the dimensionless groups to place their experiments on the regime map. They all used glass ballotini ($d_{32} \geq 27.9$ μm), so these data may fit in the Spreading/Crater Formation regime with more information. Agland and Iveson observed drop impact behavior that they divided into sink, "penetration," "clump," "spread," and "splash/breakage" regimes.[20] These mechanisms all seem similar to Spreading/Crater Formation with the exception of sink, which seems more like Tunneling. However, no images were provided to confirm the exact mechanisms. The high-speed video images along with granule images of Marston et al.[21] clearly indicate Spreading/Crater Formation behavior. Delon et al.'s high-speed video images of high-velocity water drops impacting glass ballotini clearly depict Crater Formation.[22]

All the relevant literature data either quantitatively or qualitatively confirm the regimes of Tunneling, Spreading, and Crater Formation.

Conclusions

The granule formation mechanism regime map presented in this article is a useful tool to design and predict wet granulation processes, in this case granules formed by single drop impact onto powder beds. Based on two key dimensionless groups involving formulation and process variables, $\varepsilon = 1 - \frac{\rho_{\text{bed}}}{\rho_{\text{p}}}$ (bed porosity) and $Bo_g^* = \frac{\gamma \cos\theta}{d_{32}^2 \rho_{\text{p}} g}$ (modified granular Bond number), the granule formation mechanism can be determined:

- Spreading and Crater Formation occur when $Bo_g^* < 65{,}000$ for all values of bed porosity below the minimum fluidization porosity, ε_{mf}. In this regime, granule shape is sensitive to liquid properties, drop diameter and drop release height, which are factors in both Re and We. The boundary between Spreading and Crater Formation is determined by We, where Crater Formation occurs for $We \geq 33$. In the Spreading regime, the granules formed are flat disks. When Crater Formation occurs, the granules are rounder with decreasing We, although the granule formation process is complex and other liquid and powder properties are also important.

- Tunneling occurs when $Bo_g^* > 65{,}000$ for all values of bed porosity. In this regime, round granules are produced (low V.A.R.'s), which is insensitive to liquid properties and drop release height. Higher bed porosity leads to lower V.A.R.'s for a given bed preparation method and powder.
- Engulfing should occur when $Bo_g^* < 65{,}000$ for all values of bed porosity above the minimum fluidization porosity, ε_{mf}. In this regime, fluidized free-flowing powders should form round granules, with a mechanism similar to Tunneling.

The regime map was compared with literature data, which fit nicely into their anticipated regimes. However, the map is not applicable to fibrous powder beds.

Literature Cited

1. Litster J, Ennis B, Lian L. *The Science and Engineering of Granulation Processes*. Dordrecht/Boston, MA: Kluwer Academic Publishers, 2004.
2. Wildeboer WJ, Koppendraaier E, Litster JD, Howes T, Meesters G. A novel nucleation apparatus for regime separated granulation. *Powder Technol*. 2007;171(2):96–105.
3. Schaafsma SH, Vonk P, Kossen NWF. Fluid bed agglomeration with a narrow droplet size distribution. *Int J Pharm*. 2000;193(2): 175–187.
4. Waldie B. Growth mechanism and the dependence of granule size on drop size in fluidized-bed granulation. *Chem Eng Sci*. 1991;46(11):2781–2785.
5. Hapgood KP. Nucleation and binder dispersion in wet granulation. Ph.D. thesis. Australia: Department of Chemical Engineering, The University of Queensland, 2000.
6. Hapgood K, Litster JD, Smith R. Nucleation regime map for liquid bound granules. *AIChE J*. 2003;49(2):350–361.
7. Iveson SM, Litster JD. Growth regime map for liquid-bound granules. *AIChE J*. 1998;44(7):1510–1518.
8. Kayrak-Talay D, Litster JD. A priori performance prediction in pharmaceutical wet granulation: testing the applicability of the nucleation regime map to a formulation with a broad size distribution and dry binder addition. *Int J Pharm*. 2011;418(2): 254–264.
9. Emady HN, Kayrak-Talay D, Schwerin WC, Litster JD. Granule formation mechanisms and morphology from single drop impact on powder beds. *Powder Technol*. 2011;212(1):69–79.
10. Nase ST, Vargas WL, Abatan AA, McCarthy JJ. Discrete characterization tools for cohesive granular material. *Powder Technol*. 2001;116(2–3):214–223.
11. Megias-Alguacil D, Gauckler L. Capillary and van der Waals forces between uncharged colloidal particles linked by a liquid bridge. *Colloid Polym Sci*. 2010;288(2):133–139.
12. Geldart D, Harnby N, Wong AC. Fluidization of cohesive powders. *Powder Technol*. 1984;37(1):25–37.
13. Kayrak-Talay D, Emady HN, Litster JD. Predicting granule size in nucleation only granulation for crater formation regime. In: *Proceedings 5th International Granulation Workshop*, Lausanne, Switzerland, 2011.
14. Xu CC, Zhu J. Prediction of the minimum fluidization velocity for fine particles of various degrees of cohesiveness. *Chem Eng Commun*. 2008;196(4):499–517.
15. Waldie B, Wilkinson D, Zachra L. Kinetics and mechanisms of growth in batch and continuous fluidized bed granulation. *Chem Eng Sci*. 1987;42(4):653–665.
16. Nefzaoui E, Skurtys O. Impact of a liquid drop on a granular medium: inertia, viscosity and surface tension effects on the drop deformation. *Exp Therm Fluid Sci*. 2012;41:43–50.
17. Lee ACS. Formation of granule nuclei under static and dynamic powder bed conditions. Ph.D. thesis. West Lafayette, IN: Mechanical Engineering, Purdue University, 2011.
18. Katsuragi H. Morphology scaling of drop impact onto a granular layer. *Phys Rev Lett*. 2010;104(21):218001.
19. Katsuragi H. Length and time scales of a liquid drop impact and penetration into a granular layer. *J Fluid Mech*. 2011;675:552–573.
20. Agland S, Iveson SM. The impact of liquid drops on powder bed surfaces. In: *CHEMECA*'99, Newcastle, Australia, 1999.
21. Marston JO, Thoroddsen ST, Ng WK, Tan RBH. Experimental study of liquid drop impact onto a powder surface. *Powder Technol*. 2010;203(2):223–236.
22. Delon G, Terwagne D, Dorbolo S, Vandewalle N, Caps H. Impact of liquid droplets on granular media. *Phys Rev E*. 2011;84(4):046320.
23. Emady HN. Single drop granule formation for regime separated granulation. Ph.D. thesis. West Lafayette, IN: Chemical Engineering, Purdue University, 2012.

Manuscript received Aug. 24, 2012.